Modeling Galactic Cosmic Rays Using Stochastic Differential Equations: A Tutorial

Juan G Alonso Guzman[1]

[1]University of Alabama in Huntsville

2024 Internatial Space Weather Camp

Contents

1 Introduction

This tutorial will cover the following topics:

- Regarding heliophysics:
  - Tracking charged particle trajectories in a prescribed electromagnetic environment.
  - Understanding fundamental concepts of charged particle motion such as gyration, magnetic moment and drifts.
  - Simulating galactic cosmic ray modulation by the heliosphere.
  - Understanding the main factors affecting the transport of energetic charged particles within the heliosphere, such as diffusion and adiabatic expansion.
- Regarding computer science/design of algorithms:
  - Numerically solving ordinary differential equations using explicit Runge-Kutta methods.
  - Numerically solving partial differential equations using the method of (stochastic) characteristics.
  - Distributed memory parallelization of computational tasks using an asynchronous, Master-Worker approach.

Unfinished codes in C++ will be provided which the students will complete with help from the project leader. Analysis of the output from the codes will be done using several plotting tools, like Python, Grace or VisIt. The goal is for students to simultaneously learn about space weather and sharpen their computational/research skills.

1.1 Galactic Cosmic Rays

Broadly speaking, cosmic rays are high-energy particles of extra-terrestrial origin. Their discovery is often attributed to Victor Hess and his 1912 balloon flight experiments, but many other scientists contributed to this feat, such as Theodor Wulf, Domenico Pacini, and Werner Kolhörster [De Angelis, 2011, Hörandel, 2013, Hess, 2018]. Their observations, and others made within Earth's atmosphere, are technically indirect and can only detect high energy particles because they must traverse a relatively dense medium. Weak particles will not make it very far and only the strongest ones end up colliding with atmospheric molecules and generating a cascade of other particles called an "air shower". Measurements of these events by ground-based detectors, like neutron monitors, are then fed into a model that calculates the energy of the original particle that started the cascade. In contrast, observations made with spacecraft are not hindered by Earth's atmosphere and can thus directly measure the particle's populations, even to relatively low energies. A

major drawback, however, is that the exposure time and detector size is extremely limited in space-based instruments.

We can divide cosmic rays into multiple subpopulations depending on their energy and origin. For example, solar energetic particles (SEPs) are cosmic rays that come from the Sun, mainly due to solar eruptions (flares or CMEs) and range in energy from 10 to 10^5 keV/nucleon. **Galactic cosmic rays** (GCRs) originate from supernovae, active galactic nuclei, quasars, and gamma-ray bursts within our galaxy and their energies range from 10^2 to 10^12 MeV/nucleon. Other important and interesting particle populations exist, such as magnetospheric particles, anomalous cosmic rays (ACRs) and pick-up ions (PUIs), but in this tutorial we will focus on modeling GCRs in a global sense, i.e. in scales of the entire heliosphere. GCRs are the predominant source of radiation outside of Earth's atmosphere [Kerr, 2013, Zeitlin et al., 2013], so understanding their transport patterns is crucial for assessing the radiation risks of long-term space exploration missions. In addition, the methods we will discuss today are directly transferable to other particle groups, so the skills introduced here can extend to many other areas of space physics research.

1.2 Stochastic Differential Equations

The modeling approach taught in this tutorial will hinge on the **Monte Carlo (MC) method** and **stochastic differential equations** (SDEs), so in this subsection we give a very fast and loose introduction to both. Although the label is occasionally stretched, the MC method, in its purest form, is simply an application of the law of large numbers, which states that for a sequence of independent, identically-distributed random variables, $\{X_i\}_{i=1}^{\infty}$, all with expectation $\mathbb{E}(X) = \mu$, then their running average will approach μ as more variables are taken into account,

$$\lim_{n\to\infty} \frac{1}{n} \sum_{i=1}^{n} X_i = \mu.$$

Even if not explicitly stated this way, every proper use of the MC method can be expressed in this way. In essence, this approach approximate the expected value of some process but simulating/sampling that process repeatedly and averaging the results.

In a nutshell, stochastic differential equations are differential equations of stochastic processes. Stochastic processes are sequences of random variables indexed by a single variable (discrete or continuous) commonly associated with time. An **Itô process** is a stochastic process, $\mathbf{X}_t$, that satisfies the following SDE,

$$d\mathbf{X}_t = \boldsymbol{\mu}_t dt + \kappa_t d\mathbf{W}_t, \tag{1}$$

for some initial condition, where $\boldsymbol{\mu}_t$ is called the drift term, κ_t is called the diffusion term, and $\mathbf{W}_t$ is a Wiener process. The solution to equation (1) is

$$\mathbf{X}_t = \mathbf{X}_0 + \int_0^t \boldsymbol{\mu}_s \, ds + \int_0^t \kappa_s \, d\mathbf{W}_s \tag{2}$$

where $\mathbf{X}_0$ is the initial state of the process. Note that both the drift and diffusion terms can be stochastic processes and even depend on $\mathbf{X}_t$ itself. If $\boldsymbol{\mu}_t = \mathbf{b}(t, \mathbf{X}_t)$ and $\kappa_t = \sigma(t, \mathbf{X}_t)$, we call $\mathbf{X}_t$ a **diffusion process**.

The terminology and mathematical notation can be overwhelming at first, but the physical interpretation should be clear. A diffusion process models the evolution of some quantity over some domain (e.g. space) and time subject to a deterministic drift term, $\mathbf{b}(t, \mathbf{x})$, which pushes the quantity throughout the domain in a predictable way, and the influence of a stochastic diffusion term, $\sigma(t, \mathbf{x})$, which shifts the position of the quantity within the domain in a random fashion. It is worth reiterating that $\mathbf{X}_t$ is a stochastic process, which means it is a probabilistic quantity and any two realizations of this process will almost certainly differ. The randomness of $\mathbf{X}_t$ is inhereted by that of $\mathbf{W}_t$ and modified by the manner in which $\mathbf{b}$ and σ could depend on the state of the process. If the drift and diffusion terms are deterministic (not stochastic) functions of time, then the expected value and variance of $\mathbf{X}_t$ are easily computed to be

$$\mathbb{E}[\mathbf{X}_t] = \int_0^t \mathbf{b}(s)\, ds, \tag{3}$$

and

$$\mathrm{Var}[\mathbf{X}_t] = \int_0^t \sigma^2(s)\, ds. \tag{4}$$

The physical interpretation of the above equations is that for drift and diffusion terms that do not depend on the current state of the process, upon averaging over many realizations of the random variable, called **random paths**, the expected trajectory of $\mathbf{X}_t$ is determined solely by the drift term, while the average deviation (squared) from that expected trajectory is dictated only by the diffusion term.

Diffusion processes are an interesting subject of study in their own right, but here we are more interested in using them as tools to help us solve **partial differential equations** (PDEs), and perhaps interpret their solutions. In particular, consider the following boundary value problem for some quantity $u : \Omega \to \mathbb{R}$,

$$\mathbf{b} \cdot \nabla u + \frac{1}{2}\left(\sigma\sigma^T\right) : \nabla^2 u = 0, \qquad u(\mathbf{x}) = f(\mathbf{x}) \quad (\forall \mathbf{x} \in \partial\Omega), \tag{5}$$

where $\mathbf{b}$ is a vector of the same dimension as the domain containing Ω and σ is a matrix that same number of rows. Under suitable (mild) conditions for the functions involved in this problem, then the solution can be expressed as

$$u(\mathbf{x}) = \mathbb{E}\left[f\left(\mathbf{X}_\tau\right) | \mathbf{X}_0 = \mathbf{x}\right] \tag{6}$$

where $\forall x \in \Omega$, $\tau = \inf\left\{t \geq 0 : \mathbf{X}_t \in \partial\Omega\right\}$ and $\mathbf{X}_t$ obeys the equation

$$d\mathbf{X}_t = \mathbf{b}(\mathbf{X}_t)dt + \sigma(\mathbf{X}_t)d\mathbf{W}_t, (t \geq 0), \tag{7}$$

with $\mathbf{X}_0 = \mathbf{x}$. In words, this means that the solution of (5) at some location $\mathbf{x}$ can be obtained as the expected value of the boundary function applied to the (time-homogenous) diffusion process given by (7) the first time it encounters the boundary, on the condition that the process starts $\mathbf{x}$.

When attempting to numerically compute the solution to (5) using (6) and (7), one can leverage the MC method, but this means simulating $\mathbf{X}_t$, i.e. numerically solving an SDE, many times and adequately averaging the results. Solving (7) numerically can be done by dicretizing the temporal range, $\mathbf{X}_n = \mathbf{X}(t_n)$, and iterating as follows,

1. Set initial conditions,
$$t_0 = 0,$$
$$\mathbf{X}_0 = \mathbf{x}.$$
2. Integrate trajectory one step at a time via the Euler-Maruyama scheme
$$t_{n+1} = t_n + \Delta t,$$
$$\mathbf{X}_{n+1} = \mathbf{X}_n + \mathbf{b}(\mathbf{X}_n)\Delta t + \sigma(\mathbf{X}_n)\Delta \mathbf{W}_n,$$
where $\mathbf{W}_n$ is a normally distributed random variable with mean 0 and variance Δt, until $\mathbf{X}_{n+1}$ crosses the boundary $\partial\Omega$.
3. Record $f(\mathbf{X}_{n+1})$.

In summary, we transformed the task of solving a PDE to repeatedly simulating an SDE until it hits the boundary of the domain and then averaging the boundary condition at these terminal locations. We call this the **MC method of stochastic characteristics**.

At this point, we have covered all the necessary material to continue with this tutorial, but be aware that there are many other useful tools and concepts within this subject. The MC method of stochastic characteristics can be extended to other PDEs, including time-dependent ones. Also, there are more accurate stochastic integration methods available, such as Miltein's scheme. In the limit without diffusion (no randomness), this approach is sometimes called the **flux-mapping method**.

2 Test-Particle Simulations

In plasma physics, charged particles move in an electro-magnetic environment according to some equations of motion that depend on the electro-magnetic fields present. Typically, these fields are themselves affected by the particle motion, and a system of equations must be solved self-consistently. The **text-particle limit** assumes that the particles of interest do not affect the background through which they propagate. Therefore, the force-fields that dictate particle motion are taken as given and do not require feedback from the particle population. This means that the usual two-way coupling of plasma physics can be reduced to a simpler one-way coupling.

2.1 Abstract Transport Equations

We can abstract the (deterministic) equations of motion for any transport model as simultaneously tracking N variables of position coordinates, $\{x_i\}_{i=1}^{N}$ and M variables of momentum coordinates, $\{p_j\}_{j=1}^{M}$ according to some prescribed evolution functions, $\{F_i\}_{i=1}^{N}$ $\{G_j\}_{j=1}^{M}$,

$$\frac{dx_i}{dt} = F_i(t, x_1, \ldots, x_N, p_1, \ldots, p_M), \quad i = 1, \ldots, N, \tag{8}$$

$$\frac{dp_j}{dt} = G_j(t, x_1, \ldots, x_N, p_1, \ldots, p_M), \quad j = 1, \ldots, M, \tag{9}$$

where t is time. These can usually be interpreted as characteristics of a $N + M + 1$-dimensional transport equation,

$$\frac{\partial f}{\partial t} + F_1 \frac{\partial f}{\partial x_1} + \cdots + F_N \frac{\partial f}{\partial x_N} + G_1 \frac{\partial f}{\partial p_1} + \cdots + G_M \frac{\partial f}{\partial p_M} = 0. \tag{10}$$

where $f(t, x_1, \ldots, x_N, p_1, \ldots, p_M)$ is the charged particle phase-space distribution function.

This connection is relevant because it reveals a duality in perspectives. In plasma physics, we are often concerned with an entire population of particles, not just a few of its constituents. However, in the test-particle approach, solving (10) for the population distribution function can be achieved by tracking the motion of its phase-space components, which in some cases represent individual particles, according to (8) and (9). From a purely mathematical point of view, this is called the **method of characteristics**, i.e. solving a D-dimensional partial differential equation (PDE) by solving a system of $D - 1$ coupled ordinary differential equations (ODEs).

2.1.1 Numerically Solving Equations of Motion

Solving ODEs, even to a high degree of accuracy, is a fairly simple and well-studied task. We use the following notation

$$\mathbf{y} = \begin{bmatrix} x_1 \\ \vdots \\ x_N \\ p_1 \\ \vdots \\ p_M \end{bmatrix}, \qquad \mathbf{H} = \begin{bmatrix} F_1 \\ \vdots \\ F_N \\ G_1 \\ \vdots \\ G_M \end{bmatrix},$$

and $\mathbf{y}_n = \mathbf{y}(t_n)$. Initial value problems are generally solved with the following approach:

1. Set initial conditions at t_0, i.e.

$$\mathbf{y}_0 = \mathbf{y}(t_0).$$

2. Integrate trajectory one step at a time,

$$t_n \to t_{n+1},$$
$$\mathbf{y}_n \to \mathbf{y}_{n+1},$$

until a fixed final time t_N.

3. Output results.

Step 2 in the outline above can take many forms. For simplicity, we will only consider explicit Runge-Kutta (RK) type methods here. Below are a few popular examples, all of which use $t_{n+1} = t_n + \Delta t$.

Euler's method: This is the simplest method to solve an ODE. It yields first-order accuracy in Δt.

$$\mathbf{y}_{n+1} = \mathbf{y}_n + \mathbf{H}(t_n, \mathbf{y}_n)\Delta t. \tag{11}$$

Midpoint method: This is a refinement of Euler's method. It yields second-order accuracy in Δt.

$$\mathbf{y}_{n+\frac{1}{2}} = \mathbf{y}_n + \mathbf{H}(t_n, \mathbf{y}_n)\frac{\Delta t}{2}, \tag{12}$$
$$\mathbf{y}_{n+1} = \mathbf{y}_n + \mathbf{H}(t_n + \frac{\Delta t}{2}, \mathbf{y}_{n+\frac{1}{2}})\Delta t. \tag{13}$$

Heun's method: This is a also refinement of Euler's method. It yields second-order accuracy in Δt.

$$\mathbf{k}_{n,1} = \mathbf{H}(t_n, \mathbf{y}_n), \tag{14}$$
$$\mathbf{k}_{n,2} = \mathbf{H}(t_n + \Delta t, \mathbf{y}_n + \mathbf{k}_{n,1}\Delta t), \tag{15}$$
$$\mathbf{y}_{n+1} = \mathbf{y}_n + [\mathbf{k}_{n,1} + \mathbf{k}_{n,2}]\,\frac{\Delta t}{2}. \tag{16}$$

RK4 method: This is perhaps the best known ODE solver. It yields fourth-order accuracy in Δt.

$$\mathbf{k}_{n,1} = \mathbf{H}(t_n, \mathbf{y}_n), \tag{17}$$
$$\mathbf{k}_{n,2} = \mathbf{H}(t_n + \frac{\Delta t}{2}, \mathbf{y}_n + \mathbf{k}_{n,1}\frac{\Delta t}{2}), \tag{18}$$
$$\mathbf{k}_{n,3} = \mathbf{H}(t_n + \frac{\Delta t}{2}, \mathbf{y}_n + \mathbf{k}_{n,2}\frac{\Delta t}{2}), \tag{19}$$
$$\mathbf{k}_{n,4} = \mathbf{H}(t_n + \Delta t, \mathbf{y}_n + \mathbf{k}_{n,3}\Delta t), \tag{20}$$
$$\mathbf{y}_{n+1} = \mathbf{y}_n + [\mathbf{k}_{n,1} + 2\mathbf{k}_{n,2} + 2\mathbf{k}_{n,3} + \mathbf{k}_{n,4}]\,\frac{\Delta t}{6}. \tag{21}$$

Keep in mind that the order of accuracy of a solver refers to how fast the error in the approximate solution (with respect to the true solution) decreases when Δt is reduced, and all solvers are innacurate when using a "large" timestep. Therefore, Δt should be small enough to ensure adequate accuracy, but not too small, so that the solver remains efficient. In other words, a balance should be struck between accuracy and speed.[1] A common practice is to employ a spatial Courant–Friedrichs–Lewy (CFL) condition by which a trajectory will not move more than a desired distance, Δx, within each step,

$$\Delta t = \alpha \frac{\Delta x}{\sqrt{F_1^2 + \cdots + F_N^2}} \tag{22}$$

where $\alpha < 1$. Other physical constraints on the timestep can be enforced as well.

2.2 Newton-Lorentz Transport

The most general transport model is the **Newton-Lorentz equations of motion** for a charged particle,

$$\frac{d\mathbf{r}}{dt} = \mathbf{v}, \tag{23}$$

$$\frac{d\mathbf{p}}{dt} = q\left(\mathbf{E} + \frac{\mathbf{v} \times \mathbf{B}}{c}\right), \tag{24}$$

where t is time, $\mathbf{r}$ is the particle's position, $\mathbf{p}$ is the particle's momentum, $\mathbf{v}$ is the particle's velocity, q is the particle's charge, c is the speed of light, and $\mathbf{E}, \mathbf{B}$ are the electric and magnetic field at $\mathbf{r}$. Equations (23)-(24) are the characteristics for the most general description for the evolution of a plasma species, called the **Vlasov-Boltzmann Transport Equation**,

$$\frac{\partial f}{\partial t} + \mathbf{v} \cdot \nabla f + q\left(\mathbf{E} + \frac{\mathbf{v} \times \mathbf{B}}{c}\right) \nabla_{\mathbf{p}} f = 0, \tag{25}$$

where $f(t, \mathbf{r}, \mathbf{p})$ is the charged particle phase-space distribution function.

2.2.1 Gyration

Using the Lorentz module, set $\mathbf{E} = 0$ and $\mathbf{B} = B_0\hat{\mathbf{z}}$. As initial conditions, set $\mathbf{r} = 0$ and $\mathbf{p} = p_x\hat{\mathbf{x}} + p_z\hat{\mathbf{z}}$. Try different parameters and plot the resulting trajectories. You should obtain something resembling Figure 1.

Here are a few ideas to consider and discuss with your group.

[1] Time-adaptive solvers exist. These schemes compare the solution for two different methods with a different order of accuracy and change Δt every specified number of steps so as to ensure a high-order accuracy without using an excessively small timestep.

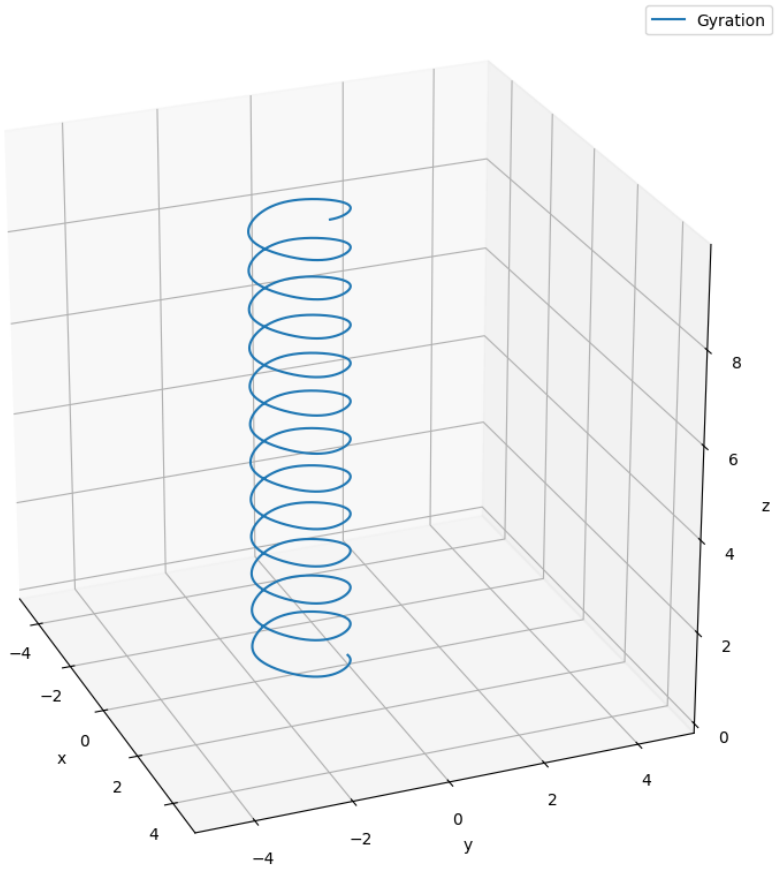

Figure 1: Gyrating motion of a charged particle in a constant magnetic field.

- The trajectory can be viewed as the composition of two motions: straightline movement parallel to $\hat{\mathbf{z}}$ and circular (periodic) motion perpendicular to $\hat{\mathbf{z}}$ (i.e. in the xy-plane). This is called **gyration** and the radius of the circles is called the **gyro-radius**. What is causing this combined movement?

- How does changing the direction/magnitude of $\mathbf{B}$ affect the trajectory?

- How does changing p_x and p_z affect the trajectory? For a valid comparison, make sure the particle energy remains constant across trials by enforcing that $\sqrt{p_x^2 + p_z^2}$ be constant.

- If you change $p_x\hat{\mathbf{x}}$ for $p_y\hat{\mathbf{y}}$ (with $p_x = p_y$) in the initial $\mathbf{p}$, would the main characteristics of the trajectory change (e.g. helix width and orientation)?

2.2.2 E x B Drift

Using the Lorentz module, set $\mathbf{E} = E_0\hat{\mathbf{x}}$ and $\mathbf{B} = B_0\hat{\mathbf{z}}$. As initial conditions, set $\mathbf{r} = 0$ and $\mathbf{p} = p_x\hat{\mathbf{x}} + p_z\hat{\mathbf{z}}$. Try different parameters and plot the resulting trajectories. You should obtain something resembling Figure 2.

Here are a few ideas to consider and discuss with your group.

- The trajectory can be viewed as the composition of two motions: the already studied gyration about the magnetic field plus a straightline drift parallel to $\hat{\mathbf{y}}$. The latter is termed $\mathbf{E} \times \mathbf{B}$ **drift**. What is causing this combined movement?

- How does changing the direction/magnitude of $\mathbf{B}$ or $\mathbf{E}$ affect the trajectory? Try to isolate the effects of simple gyration, studied previously, and the drift.

- How does changing p_x and p_z affect the trajectory? For a valid comparison, make sure the particle energy remains constant across trials by enforcing that $\sqrt{p_x^2 + p_z^2}$ be constant.

- If you change $p_x\hat{\mathbf{x}}$ for $p_y\hat{\mathbf{y}}$ (with $p_x = p_y$) in the initial $\mathbf{p}$, would the main characteristics of the trajectory change (e.g. direction of the drift)?

2.2.3 Magnetic Mirroring and Other Drifts

Using the Lorentz module, set $\mathbf{E} = 0$ and make the magnetic field a dipole in the $\hat{\mathbf{z}}$ direction,

$$\mathbf{B} = B_0 \left(\frac{3z}{r^2}\mathbf{r} - \hat{\mathbf{z}} \right). \tag{26}$$

As initial conditions, set $\mathbf{r} = x_0\hat{\mathbf{x}}$ and $\mathbf{p} = p_x\hat{\mathbf{x}} + p_z\hat{\mathbf{z}}$. Try different parameters and plot the resulting trajectories. You should obtain something resembling Figure 3.

Here are a few ideas to consider and discuss with your group.

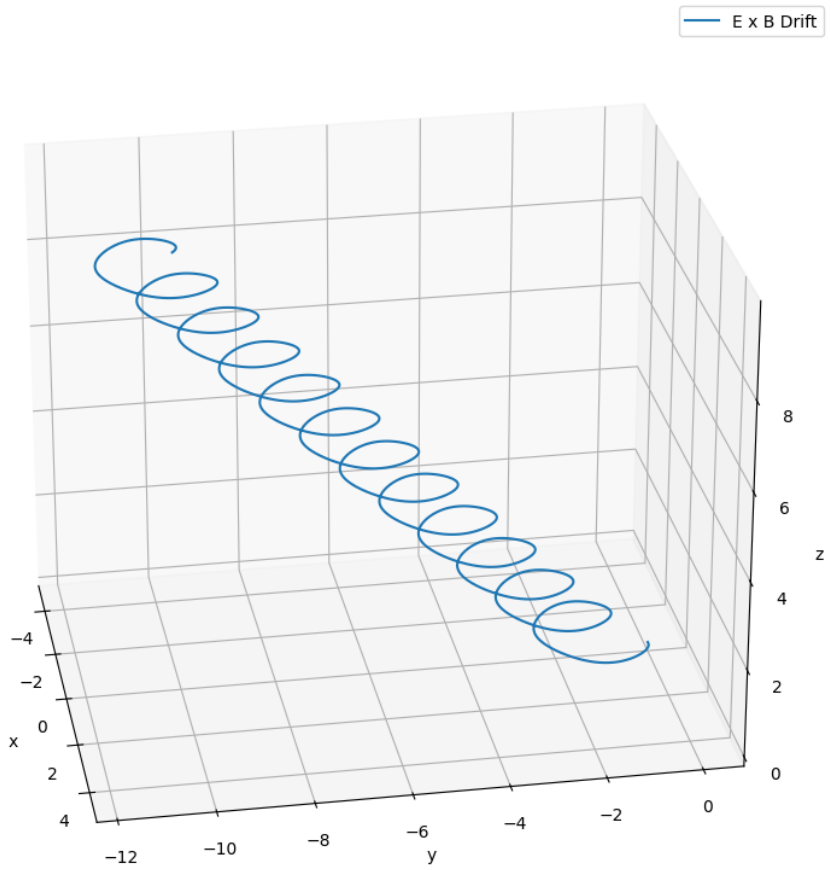

Figure 2: Gyrating and drifting motion of a charged particle in a constant magnetic field and electric field perpendicular to each other.

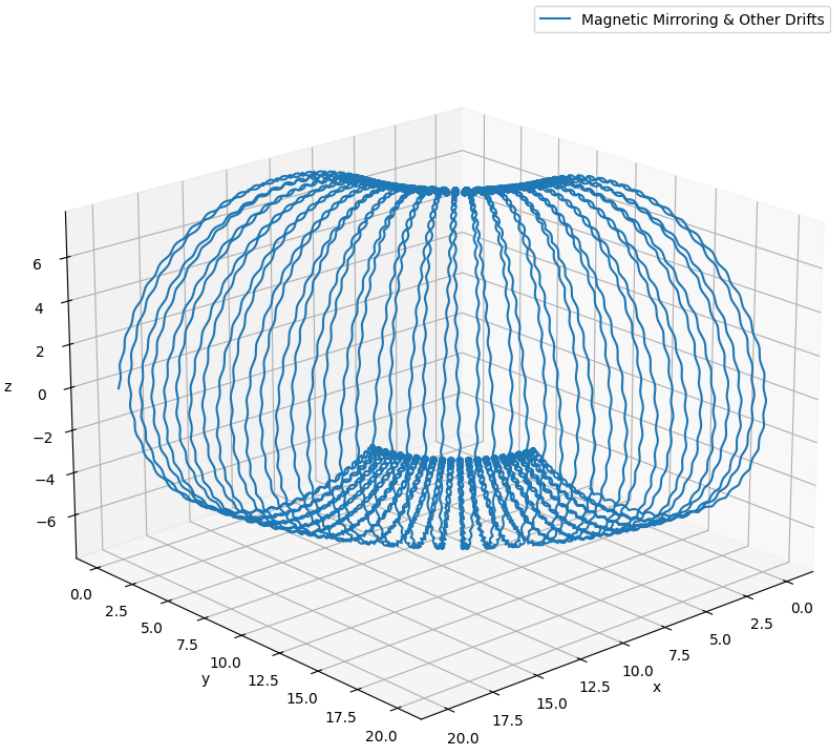

Figure 3: Motion of a charged particle in a dipole magnetic field.

- The trajectory can be viewed as the composition of multiple motions. At the smallest scale, we can see gyration about the magnetic field lines of the dipole. At an intermediate scale, the trajectory also bounces between the north and south poles (this is called **magnetic mirroring**). Finally, at the largest scale, there is a circular drift of the particle around the dipole axis. What is causing these motions? You should discover two new drifts: the **gradient drift** and the **curvature drift**.
- How does changing the parameter B_0 affect the trajectory?
- How does changing p_x and p_z affect the trajectory? For a valid comparison, make sure the particle energy remains constant across trials by enforcing that $\sqrt{p_x^2 + p_z^2}$ be constant.
- If you change $p_x\hat{\mathbf{x}}$ for $p_y\hat{\mathbf{y}}$ (with $p_x = p_y$) in the initial $\mathbf{p}$, would the main characteristics of the trajectory change?

2.2.4 Shock Drift Acceleration

Using the Lorentz module, set $\mathbf{E} = E_0\hat{\mathbf{y}}$ and

$$\mathbf{B} = \begin{cases} B_0\hat{\mathbf{z}}, & x \leq 0, \\ 2B_0\hat{\mathbf{z}}, & x > 0. \end{cases} \tag{27}$$

As initial conditions, set $\mathbf{r} = -x_0\hat{\mathbf{x}}$ and $\mathbf{p} = p_y\hat{\mathbf{y}}$. Try different parameters and plot the resulting trajectories. You should obtain something resembling Figure 4.

Here are a few ideas to consider and discuss with your group.

- For some context, this setup mimics an idealized **perpendicular MHD shock**. The plasma flow oriented along the $\hat{\mathbf{x}}$ direction is carrying a magnetic field parallel to $\hat{\mathbf{z}}$ when it encounters a shock at $x = 0$. The shock strength is 2, which means that, by the Rankine-Hugoniot conditions, the flow velocity decreased by a factor of 2 and the magnetic field increases by that same factor. Assuming a plasma of infinite conductivity, this plasma generates a **motional electric field** in the $\hat{\mathbf{y}}$ direction with magnitude proportional to the products of the plasma flow speed and magnetic field strength. Since the plasma flow speed and strength of the magnetic field decrease and increase, respectively, by the same amount, the magnitude of the electric field on either side of the shock is the same.
- The trajectory seems to have three main stages. First, it gyrates and drifts along $\hat{\mathbf{x}}$. When it encounters the shock, the motion is combined with a drift parallel to the shock. Finally, when the particle's gyroradius does not intersect the shock anymore, the particle returns to gyrating and drift only along $\hat{\mathbf{x}}$. Describe these motions in terms of the drifts you've already explored.

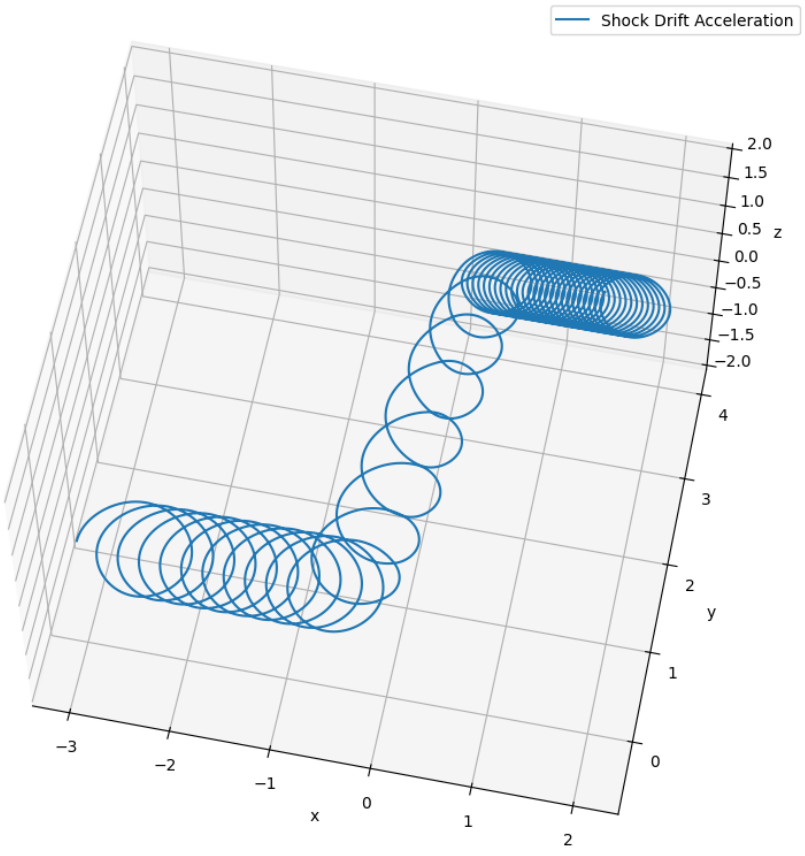

Figure 4: Motion of a charged particle encountering a perpendicular MHD shock.

- Plot the particle's energy $\sqrt{p_x^2 + p_y^2 + p_z^2}$ as a function of time. What do you notice happens before, during, and after the shock? You should discover **shock drift acceleration**.

2.2.5 Current Sheet Drift

Using the Lorentz module, set $\mathbf{E} = 0$ and

$$\mathbf{B} = \begin{cases} B_0\hat{\mathbf{z}}, & x \leq 0, \\ -B_0\hat{\mathbf{z}}, & x > 0. \end{cases} \tag{28}$$

As initial conditions, set $\mathbf{r} = 0$ and $\mathbf{p} = p_x\hat{\mathbf{x}}$. Try different parameters and plot the resulting trajectories. You should obtain something resembling Figure 5.

Here are a few ideas to consider and discuss with your group.

- For some context, this setup mimics an idealized **current/neutral sheet**. A magnetic field parallel to $\hat{\mathbf{z}}$ reversed (i.e. changes sign but keeps its magnitude) when it encounters a discontinuity at $x = 0$. Ampere's Law dictates that a current density will appear on the surface separating the regions of opposite polarity, hence the name "current sheet". In reality, the magnetic field magnitude would severely decrease along this boundary ($B \approx 0$), which explains the alternative name "neutral sheet".
- The trajectory is clearly drifting along the current sheet. Why? This is called **current sheet drift**.
- How does changing the parameters B_0 or p_x affect the trajectory?
- How does changing $\mathbf{r}$ or the direction of $\mathbf{p}$ affect the trajectory?

2.3 Guiding Center Transport

By averaging trajectories over gyroradius, one can obtain the **Hamiltonian guiding center equations of motion** for a charged particle,

$$\frac{d\mathbf{r}_g}{dt} = \frac{1}{\mathbf{B}^* \cdot \mathbf{b}} \left(\frac{p_\parallel}{\gamma m} \mathbf{B}^* + c\mathbf{E}^* \times \mathbf{b} \right), \tag{29}$$

$$\frac{dp_\parallel}{dt} = \frac{q\mathbf{E}^* \cdot \mathbf{B}^*}{\mathbf{B}^* \cdot \mathbf{b}}, \tag{30}$$

$$\frac{dp_\perp}{dt} = \frac{p_\perp}{2B} \frac{\mathrm{d}B}{\mathrm{d}t}, \tag{31}$$

where t is time, $\mathbf{r}_g$ is the particle's guiding center, $p_\parallel$ is the particle's parallel component of momentum, $p_\perp$ is the particle's perpendicular component of momentum,[2] γ is the rel-

[2]The momentum space coordinate axes are aligned with the magnetic field at $\mathbf{r}_g$ in the observer/rest frame.

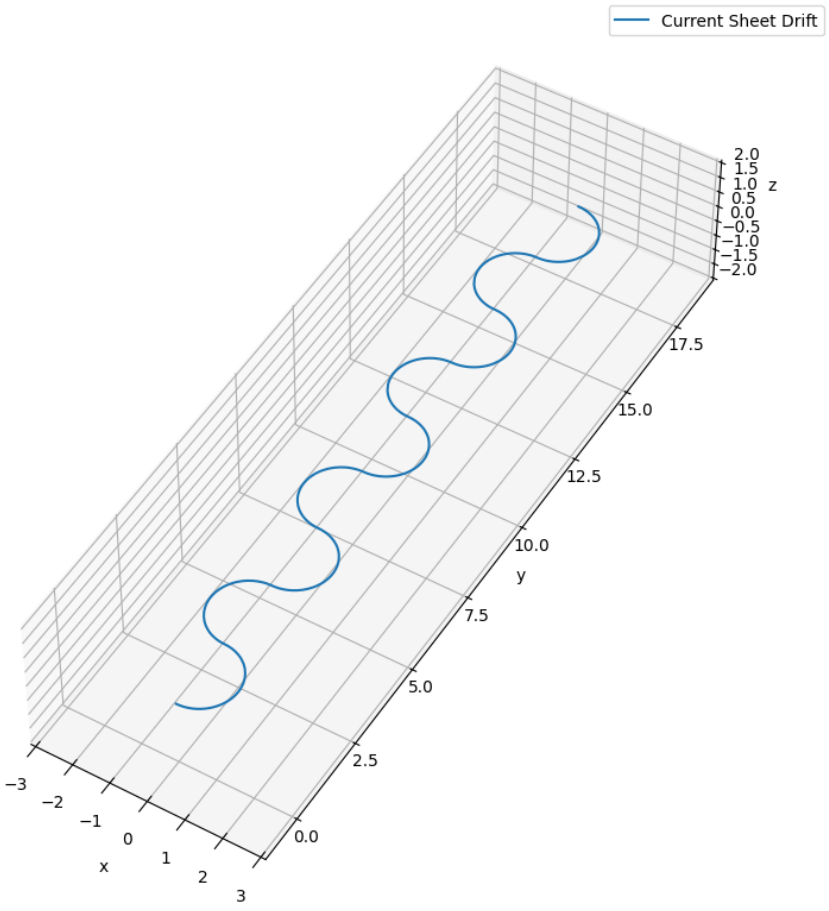

Figure 5: Motion of a charged particle encountering a current/neutral sheet.

ativistic Lorentz factor, m is the particle's rest mass, q is the particle's charge, $\mathbf{E}$ and $\mathbf{B}$ represent the electric and magnetic fields at $\mathbf{r}_g$, B is the magnitude of $\mathbf{B}$, $\mathbf{b} = \mathbf{B}/B$, and

$$\frac{\mathrm{d}B}{\mathrm{d}t} = \frac{\partial B}{\partial t} + \frac{1}{\mathbf{B}^* \cdot \mathbf{b}} \left(\frac{p_\parallel}{\gamma m} \mathbf{B}^* + c\mathbf{E}^* \times \mathbf{b} \right) \cdot \nabla_g B.$$

The modified electromagnetic fields are

$$\mathbf{E}^* = \mathbf{E} - \frac{1}{q} \left(p_\parallel \frac{\partial \mathbf{b}}{\partial t} + \frac{p_\perp^2}{2\gamma m B} \nabla_g B \right), \tag{32}$$

$$\mathbf{B}^* = \mathbf{B} + \frac{p_\parallel c}{q} \nabla_g \times \mathbf{b}. \tag{33}$$

Equations (29)-(31) are the characteristics for the **Guiding Center Transport Equation**, applicable the limit of a weakly non-uniform, slowly varying electromagnetic background,[3]

$$\frac{\partial f}{\partial t} + \frac{1}{\mathbf{B}^* \cdot \mathbf{b}} \left(\frac{p_\parallel}{\gamma m} \mathbf{B}^* + c\mathbf{E}^* \times \mathbf{b} \right) \cdot \nabla_g f + \left(\frac{q\mathbf{E}^* \cdot \mathbf{B}^*}{\mathbf{B}^* \cdot \mathbf{b}} \right) \frac{\partial f}{\partial p_\parallel} + \left(\frac{p_\perp}{2B} \frac{\mathrm{d}B}{\mathrm{d}t} \right) \frac{\partial f}{\partial p_\perp} = 0, \tag{34}$$

where $f(t, \mathbf{r}_g, p_\parallel, p_\perp)$ is the particle distribution function. Equation (34) does not have any diffusion terms, and hence its characteristics are purely deterministic. Both perpendicular diffusion and pitch-angle scattering can be incorporated into this model, but these are out of the scope of this tutorial.

2.4 Focused Transport

Another popular set of equations in this context, with a comparable level of complexity as the previous model, is the **focused transport equations of motion** for a charged particle without pitch-angle diffusion,

$$\frac{d\mathbf{r}}{dt} = \mathbf{u} + v\mu\mathbf{b}, \tag{35}$$

$$\frac{dp}{dt} = \frac{p}{2} \left[(1 - 3\mu^2)\mathbf{bb} : \nabla\mathbf{u} - (1 - \mu^2)\nabla \cdot \mathbf{u} - \frac{2\mu}{v} \mathbf{b} \cdot \frac{\mathrm{d}\mathbf{u}}{\mathrm{d}t} \right], \tag{36}$$

$$\frac{d\mu}{dt} = \frac{1 - \mu^2}{2} \left(v\nabla \cdot \mathbf{b} - 3\mu\mathbf{bb} : \nabla\mathbf{u} + \mu\nabla \cdot \mathbf{u} - \frac{2}{v} \mathbf{b} \cdot \frac{\mathrm{d}\mathbf{u}}{\mathrm{d}t} \right), \tag{37}$$

where t is time, $\mathbf{r}$ is the particle's position, p is the particle's momentum magnitude, μ is the particle's pitch-angle cosine, v is the particle speed, $\mathbf{u}$ is the background plasma flow

[3] Specifically, this means $r_L \ll L$ and $\Omega_c^{-1} \ll T$, where r_L and Ω_c are the particle's Larmor radius and cyclotron frequency, respectively, while L and T are the characteristic length and timescales of the fields variations.

velocity at $\mathbf{r}$, $\mathbf{b}$ is the unit vector in the direction of the magnetic field at $\mathbf{r}$, $D_{\mu\mu}$ is the pitch-angle scattering coefficient, and

$$\frac{\mathrm{d}\mathbf{u}}{\mathrm{d}t} = \frac{\partial \mathbf{u}}{\partial t} + \mathbf{u}\cdot\nabla\mathbf{u}.$$

Note that v and p are measured in the plasma flow frame, while μ and $\mathbf{b}$ are taken at the particle's current position. Equations (35)-(37) are the characteristics for the **Focused Transport Equation**, valid under the assumption of gyrotropy in the plasma flow frame (where the electric field is zero),

$$\begin{aligned}\frac{\partial f}{\partial t} + (\mathbf{u} + v\mu\mathbf{b})\cdot\nabla f + \frac{p}{2}\left[(1-3\mu^2)\mathbf{bb}:\nabla\mathbf{u} - (1-\mu^2)\nabla\cdot\mathbf{u} - \frac{2\mu}{v}\mathbf{b}\cdot\frac{\mathrm{d}\mathbf{u}}{\mathrm{d}t}\right]\frac{\partial f}{\partial p} \\ + \frac{1-\mu^2}{2}\left[v\nabla\cdot\mathbf{b} - 3\mu\mathbf{bb}:\nabla\mathbf{u} + \mu\nabla\cdot\mathbf{u} - \frac{2}{v}\mathbf{b}\cdot\frac{\mathrm{d}\mathbf{u}}{\mathrm{d}t}\right]\frac{\partial f}{\partial \mu} = 0,\end{aligned} \tag{38}$$

where $f(t,\mathbf{r},p,\mu)$ is the gyrophase averaged distribution function. Pitch-angle scattering is commonly included in this model, although it is omitted here for simplicity.

2.5 Parker Transport

Finally, a prefered model for helio and astrophysics applications due to its simplicity is the **Parker characteristic equations**,

$$\frac{d\mathbf{r}}{dt} = \mathbf{u} + \mathbf{v}_D + \mathbf{K}, \tag{39}$$

$$\frac{dp}{dt} = -p\frac{\nabla\cdot\mathbf{u}}{3}, \tag{40}$$

where t is time, $\mathbf{r}$ is the particle's position, p is the particle's momentum magnitude, $\mathbf{u}$ is the background plasma flow velocity at $\mathbf{r}$, and $\mathbf{v}_D$ incorporates the gradient and curvature magnetic field drifts in a compact form,

$$\mathbf{v}_D = \frac{pvc}{3q}\nabla\times\left(\frac{\mathbf{B}}{B^2}\right), \tag{41}$$

where v is the particle speed, q is the particle's charge, c is the speed of light, $\mathbf{B}$ is magnetic field at $\mathbf{r}$, and B is the magnitude of $\mathbf{B}$. The term $\mathbf{K}$ comes from solving the stochastic equation

$$d\mathbf{K} = -\left(\nabla\cdot\kappa\right)dt + \sigma d\mathbf{W}_t, \tag{42}$$

where κ is the (symmetric) diffusion tensor at $\mathbf{r}$, $\mathbf{W}_t$ is a 3D Wiener process, and $\sigma\sigma^T = 2\kappa$. This equation is simultaneously solved and the result added to (39) at each step. It is worth highlighting that (39)-(42) do not describe single particle motion. Instead, these are the

characteristics for the **Parker Transport Equation**, valid for nearly isotropic description of plasma,

$$\frac{\partial f}{\partial t} + (\mathbf{u} + \mathbf{v}_D) \cdot \nabla f - \nabla \cdot (\kappa \cdot \nabla f) - p \frac{\nabla \cdot \mathbf{u}}{3} \frac{\partial f}{\partial p} = 0, \tag{43}$$

where $f(t, \mathbf{r}, p)$ is the pitch-angle averaged distribution function. The correspondence between (43) and (39)-(42) becomes apparent when considering

$$\nabla \cdot (\kappa \cdot \nabla f) = (\nabla \cdot \kappa) \cdot \nabla f + \kappa : \nabla^2 f.$$

The effect of spatial diffusion must be included in this type of transport, so we account for it in this tutorial. A general form for κ, is

$$\kappa_{ij} = \kappa_\perp \delta_{ij} + \left(\kappa_\parallel - \kappa_\perp\right) b_i b_j, \tag{44}$$

where $\kappa_\parallel$ and $\kappa_\perp$ are the (locally) parallel and perpendicular (to $\mathbf{B}$) components of diffusion, respectively, $\mathbf{b} = \mathbf{B}/B$, and δ is the identity tensor. When using a reference frame that is locally aligned to the magnetic field, meaning $\mathbf{b} = \hat{\mathbf{z}}$, then

$$\kappa = \begin{pmatrix} \kappa_\perp & 0 & 0 \\ 0 & \kappa_\perp & 0 \\ 0 & 0 & \kappa_\parallel \end{pmatrix}, \quad \text{and} \quad \sigma = \begin{pmatrix} \sqrt{2\kappa_\perp} & 0 & 0 \\ 0 & \sqrt{2\kappa_\perp} & 0 \\ 0 & 0 & \sqrt{2\kappa_\parallel} \end{pmatrix}.$$

2.6 Investigating Numerical Methods

Since we relying on an algorithm to solve the equations of motion in our test-particle simulations, we should investigate the reliability of these tools. In particular, we can explore the accuracy of the methods used in the time-stepping procedure as a function of the simulation parameters. Pick one of the numerical experiments from Subsection 2.2 and study how the trajectories change with the CFL condition or maximum Δx for various time-stepping methods.

3 Modulation Simulations

In this section, we will solve equation (43) in the context of GCR heliospheric modulation by using the method of stochastic characteristics via (39)-(42). For this application, we will consider the steady-state version of (43), i.e. $\partial f/\partial t = 0$, which makes this a boundary value problem.

The general outline of the simulation will be as follows:

1. Initialize distribution arrays.
2. Loop over total number of pseudo-trajectories to simulate:

i) Set initial conditions.

$$\begin{aligned} t_0 &= 0, \\ \mathbf{r}_0 &= r_{in}\hat{\mathbf{x}}, \\ p_0 &= LU[p_{min}, p_{max}], \end{aligned}$$

where LU is a logarithmically uniform random number between p_{min} and p_{max}.

ii) Integrate the trajectory using (for simplicity) the Euler-Maruyama scheme,

$$\begin{aligned} t_{n+1} &= t_n + \Delta t, \\ \mathbf{r}_{n+1} &= \mathbf{r}_n - \left[\mathbf{u}(\mathbf{r}_n) + \mathbf{v}_D(\mathbf{r}_n) - \nabla\cdot\kappa(\mathbf{r}_n)\right]\Delta t \\ &\quad + \left[\mathbf{b}_{\perp,1}\sqrt{2\kappa_\perp}W_{n,1} + \mathbf{b}_{\perp,2}\sqrt{2\kappa_\perp}W_{n,2} + \mathbf{b}\sqrt{2\kappa_\parallel}W_{n,3}\right]\sqrt{\Delta t}, \\ p_{n+1} &= p_n + p_n\frac{\nabla\cdot\mathbf{u}(\mathbf{r}_n)}{3}\Delta t, \end{aligned}$$

until a boundary is crossed. In the above notation, $\mathbf{b}_{\perp,1}$ and $\mathbf{b}_{\perp,2}$ are two mutually orthogonal unit vectors that are also perpendicular to $\mathbf{b}$ and $W_{n,1}, W_{n,2}, W_{n,3}$ are three independent, normally-distributed random variables.

iii) Bin trajectory in distribution arrays according to the initial/final values.

3. Output distribution arrays.

3.1 A Simple Program

In this first attempt, we will approximate the heliosphere as spherical, with radius R_H, and centered at the Sun. The solar wind flow and magnetic field will both be radial and flowing out from the Sun,

$$\begin{aligned} \mathbf{u} &= u_0\hat{\mathbf{r}}, \\ \mathbf{B} &= B_0\hat{\mathbf{r}}. \end{aligned}$$

This implies that we can ignore the magnetic drift term, i.e. $\mathbf{v}_D = 0$. The diffusion tensor, κ, will be isotropic and linear with radial distance from the Sun

$$\kappa_\parallel = \kappa_\perp = \kappa_0\left(\frac{r}{r_0}\right). \tag{45}$$

We also assume the distribution function at the outer boundary is uniform in space and is inversely proportional to the square of momentum,

$$f(R_H, p) = f_0\left(\frac{p_0}{p}\right)^2. \tag{46}$$

This implies that the density of the GCR population is inversely proportional to their energy. In other words, there are less high energy GCRs than low energy GCRs, which is sensible. We will solve the equation for a range of radial distances from 1 au (Earth) to 80 au (outer boundary) and a range of kinetic energies from 10 MeV to 5 GeV. You should obtain something resembling Figure 6.

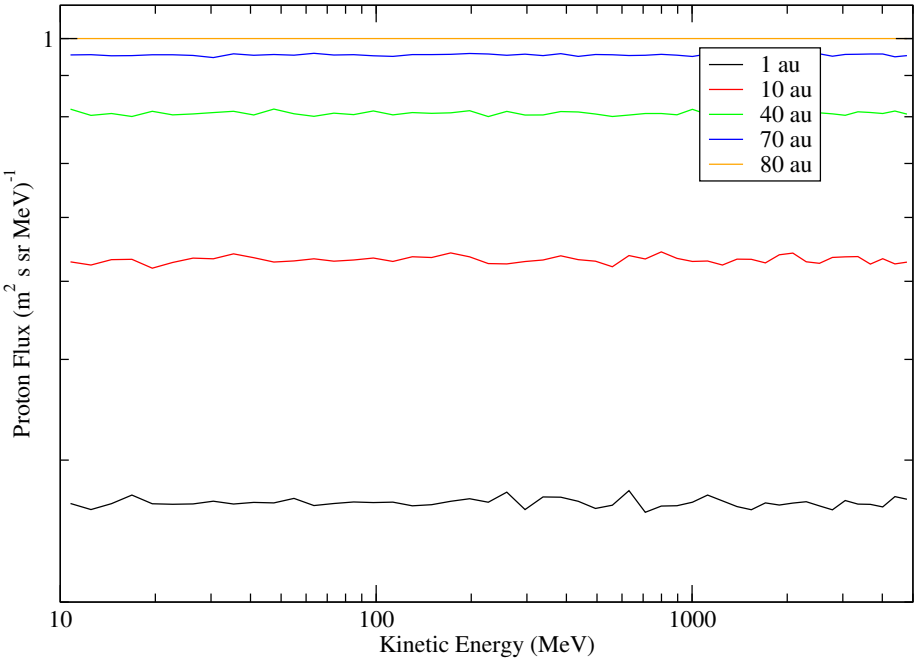

Figure 6: Computed modulated spectra for the simple model from §3.1. The parameters used were $u_0 = 400\,\mathrm{km\,s}$, $B_0 = 5\,\mathrm{nT}$ $\kappa_0 = 1.5 \times 10^{21}\,\mathrm{cm^2\,s}$, $r_0 = 1\,\mathrm{au}$, and $f_0 = p_0^{-2}$.

Here are a few ideas to consider and discuss with your group.

- The spectra appear to diminish in intensity closer to the Sun. Is this reasonable and to what do you attribute this effect?
- The spectra seem to be mostly constant in energy. Is this reasonable and why does the simulation produce constant curves?
- The spectra also appear a bit "noisy". To what do you attribute the noise in the results?

3.2 Adding Complexity

For a slightly more realistic simulation, we will follow [Fisk and Axford, 1969]. In this case, the diffusion coefficient, still isotropic, will have a quadratic function of radial distance and a linear function of kinetic energy,

$$\kappa_{\parallel}(r,T) = \kappa_{\perp}(r,T) = \kappa_0 \left(\frac{r}{r_0}\right)^2 \left(\frac{T}{T_0}\right), \tag{47}$$

meaning that diffusion is more efficient farther from the Sun and for higher energy particles. In addition, the boundary condition will still be uniform in space but will now depend on kinetic energy. In the original paper, this was enforced by making differential density a decreasing power-law, but for our purposes this translates to

$$f(R_H,T) = \frac{J_0}{p^2}\left(\frac{v}{c}\right)\left(\frac{T}{T_0}\right)^{\alpha}. \tag{48}$$

The differential (kinetic energy) density, U_T, is connected to the distribution function through the differential (kinetic energy) intensity, J_T via

$$\frac{vU_T}{8\pi} = J_T = p^2 f.$$

You should obtain something resembling Figure 7.

An even more realistic model uses a Parker spiral magnetic field [Parker, 1958], given in spherical coordinates by

$$B_r = B_0\left(\frac{r_0}{r}\right)^2, \tag{49}$$

$$B_\theta = 0,$$

$$B_\phi = -B_r\left(\frac{\Omega}{u_0}\right) r\sin(\theta), \tag{50}$$

where Ω is the angular rotation frequency of the Sun and r_0 is the radius at which the solar wind can be approximated as radial. Although magnetic drifts are very much not negligible in this field configuration, assume $\mathbf{v}_D = 0$ for simplicity. We expect diffusion to be much more efficient along the magnetic field than across it [Mace et al., 2000], and also to be inversely proportional to magnetic field strength, so we will try

$$\kappa_{\parallel}(B,p) = \frac{\lambda v}{3}\frac{B_0}{B}\sqrt{\frac{p}{p_0}}, \quad \text{and} \quad \kappa_{\perp} = \eta\kappa_{\parallel}, \tag{51}$$

where λ represents the mean free path of diffusive events, and $\eta < 1$ is the ratio of perpendicular to parallel diffusion. Finally, we can use the differential intensity measured by

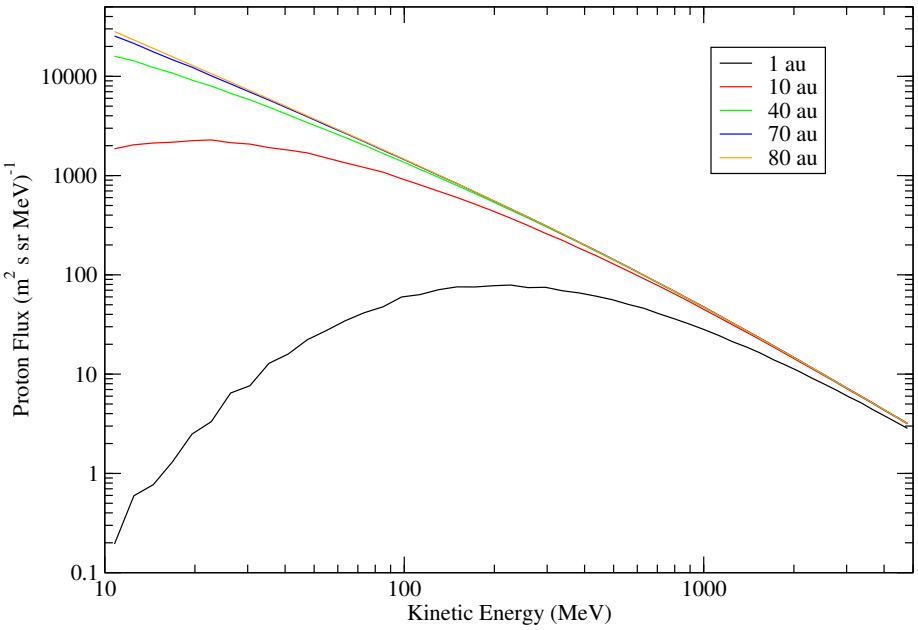

Figure 7: Computed modulated spectra for the model from [Fisk and Axford, 1969]. The parameters used were $u_0 = 400\,\mathrm{km\,s}$, $B_0 = 5\,\mathrm{nT}$, $\kappa_0 = 1.5 \times 10^{21}\,\mathrm{cm^2\,s}$, $r_0 = 1\,\mathrm{au}$, $T_0 = 1\,\mathrm{GeV}$, $J_0 = 54\,\mathrm{m^{-2}\,s^{-1}\,sr^{-1}\,MeV^{-1}}$, and $\alpha = -1.8$.

the Voyager spacecraft [Cummings et al., 2016] to model the outer boundary condition as a bent power-law,

$$f(R_H, T) = \frac{J_0}{p^2} \frac{\left(\frac{T}{T_0}\right)^{\alpha_1}}{\left[1 + \left(\frac{T}{T_b}\right)^{\alpha_2/d}\right]^d}, \tag{52}$$

where T_b is the bendover energy and α_1 and α_2 are the slopes before and after the bend, respectively, and d controls the sharpness of the bend. You should obtain something resembling Figure 8.

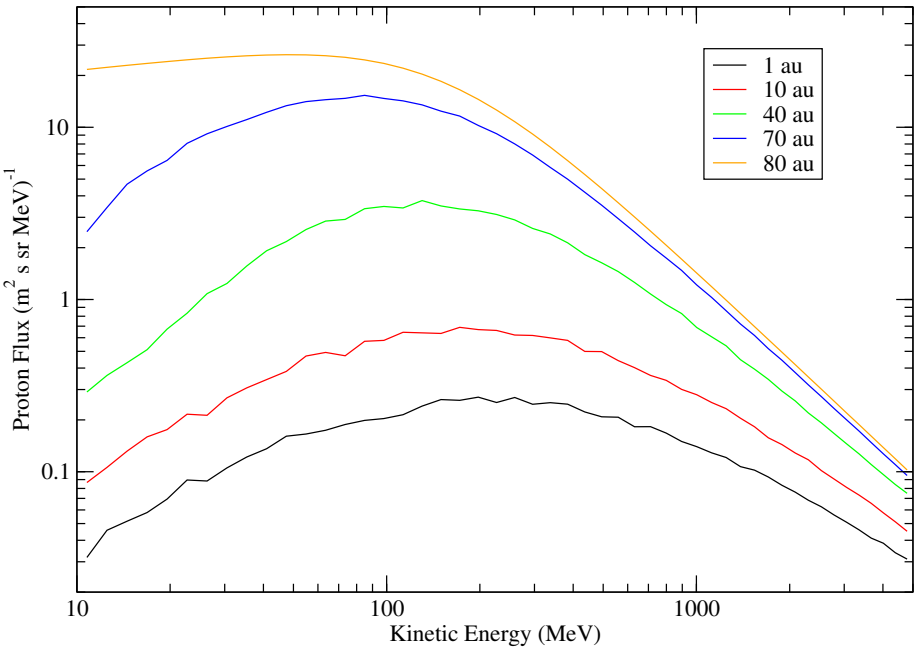

Figure 8: Computed modulated spectra for the "more realistic" model from §3.2. The parameters used were $u_0 = 400\,\mathrm{km\,s}$, $B_0 = 5\,\mathrm{nT}$, $r_0 = 1\,\mathrm{au}$, $\Omega = 2\pi/25\,\mathrm{days}^{-1}$, $\lambda = 0.05\,\mathrm{au}$, p_0 is the momentum of a proton with 1 GeV kinetic energy, $\eta = 0.1$, $J_0 = 54\,\mathrm{m}^{-2}\,\mathrm{s}^{-1}\,\mathrm{sr}^{-1}\,\mathrm{MeV}^{-1}$, $T_0 = 1\,\mathrm{GeV}$, $T_b = 150\,\mathrm{MeV}$, $\alpha_1 = 0.2$, $\alpha_2 = 1.9$ and $d = 1$.

If you are interested in capturing the magnetic drift effects in this model, you'll have to incorporate Equation (41) into the code using finite differences. In addition, in order to obtain the correct global drift pattern, you'll have specify a heliospheric current sheet (HCS) topology and ensure the field polarity is reversed across it. The simplest HCS model is a flat neutral surface at the equator ($\theta = \pi/2$), with the sign of $\mathbf{B}$ "manually" flipped either north or south of it. The magnitude of $\mathbf{v}_D$ can become unphysically high (larger

than c) near the current sheet and the polar regions, so it can be artificially limited by a reasonable upper bound ($c/2$).

Here are a few ideas to consider and discuss with your group.

- The spectra vary with energy in a non-linear fashion. Specifically, lower energy particles seem to be more modulated than high energy particles. Is this reasonable and to what do you attribute this effect?
- How does changing the mean free path parameter, λ, affect the results?
- How does changing the anistropy parameter, η, affect the results?

3.3 Comparing to Observations

Figure 9 shows time-averaged proton fluxes, J_T, as functions of particle kinetic energy at different times between 2010 and 2014 measured by the PAMELA instrument on-board an Earth orbiting satellite [Martucci et al., 2018]. Your task will be to attempt to match these observations by varying the parameters of the previous model. You'll have to first fit the Voyager measurements along with the high energy ($> 10\,\mathrm{GeV}$) PAMELA observations using Equation (52).

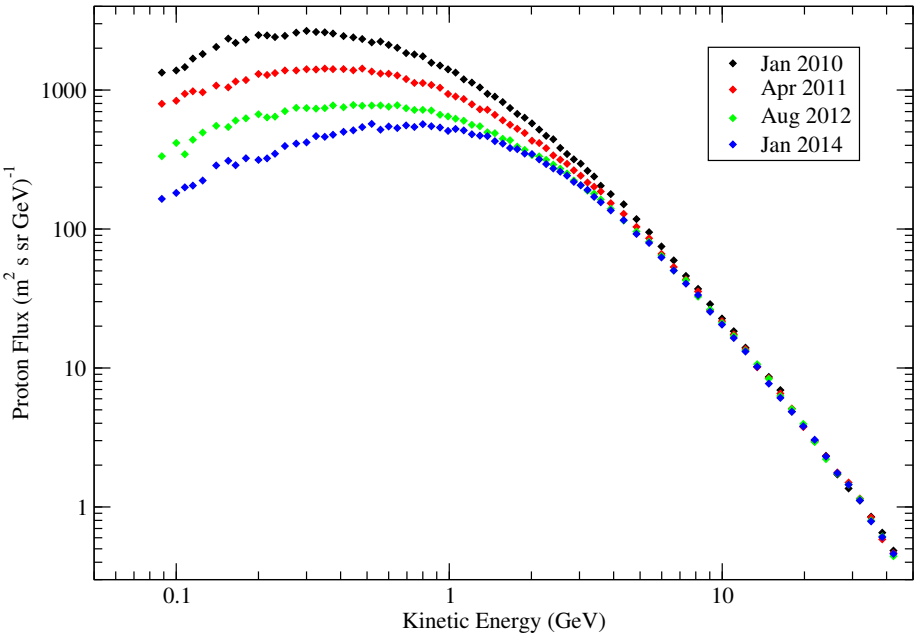

Figure 9: Proton fluxes during four 1 month-intervals of the PAMELA mission.

3.4 Parallelization

In order to speed up the simulation, we will parallelize it using an asynchronous, Master-Worker model. In this scheme, a single processor (the "Master") will assign batches of trajectories to the rest of CPUs in the system (the "Worker(s)"). The workers will integrate all of their assigned trajectories, each keeping track of a partial distribution which they will communicate to the master at the end of the simulation. The "asynchronous" feature means that the workers do not need to coordinate amongst themselves. They each interact with the master independently and will finish their assigned tasks at different times.

The general outline of the simulation will be as follows:

1. All processor initialize distribution arrays.
2. The master partitions the work and communicates the assigned tasks to each worker.
3. The workers independently perform their work, collecting partial results. Keep in mind that the master can also do some of the work.
4. The master collects all of the partial distributions into a cumulative distribution, and outputs it.

3.5 Investigating Numerical Methods

The MC algorithm used to solve the transport equations in this section produces results that are not smooth when visualized. The noise in the graphs is related to the uncertainty in the solution, meaning we are more confident about a smoother result. Like in any MC method, uncertainty is reduced, and thus graphs can be made smoother, by using a larger number of sample trajectories. One could artificially smooth the graph in post-processing as well. Compare both ways of obtaining smoother results.

When code execution is parallelized, there are unavoidable overhead costs related to the communication between the CPUs. To investigate the efficiency of a parallelization scheme we look at two main scaling properties. **Strong scaling** refers to how the execution time of a program varies with the number of processors for a fixed problem size.[4] **Weak scaling** refers to how the execution time of a program varies with the number of processors for a fixed problem size *per processor*. Perfect strong scaling would mean that the execution time is inversely proportional to the number of processors, while perfect weak scaling gives a constant execution time. Explore the strong/weak scaling for our parallelization scheme.

[4] The problem size in our applications is the number of psuedo-trajectories to integrate.

A Linux Primer

Here is a quick introduction to some linux terminal commands that will be useful to you as you compile and run the C/C++ codes in this tutorial.

- `man` This commands pull up a manual for any other command. For example,

  ```
  user@host $> man g++
  ```

  will pull up a manual for the `g++` command.

- `history` This commands prints all the previous commands executed within the current session, even those that were incorrect. It can help find a command you ran previously if you forget the specific syntax.

- `pwd` This commands prints the path to the current directory. It's useful to figure out where the heck you are if you're lost within the file system.

- `ls` This commands lists all the contents of the current directory. It can be used with a combination of flags which give more detailed information about the contents of the directory. For example,

  ```
  user@host $> ls -alh
  ```

  will list ALL the files (`-a`), including "hidden" ones, one item per line (`-l`) along with owner, accessibility, and size information in human readable format (`-h`).

- `cd` This command allows you to change your current directory. In particular, you can change to the home directory with

  ```
  user@host $> cd
  ```

  the current parent directory with

  ```
  user@host $> cd ..
  ```

  and previous directory with

  ```
  user@host $> cd -
  ```

- `less` This command lets you preview the first few lines of a file, and offer a rudimentary file navigation interface through the terminal. It can be useful to check whether the code output is reasonable before attempting to plot it.

- `cp` This command lets you make a copy of an existing file. For example,

```
user@host $> cp file1.txt file2.txt
```

  will copy file `file1.txt` and name the copy `file2.txt`. If you want to copy a directory, use the `-r` flag.

- `mv` This command lets you move the location of a file or empty directory, potentially renaming it in the process. For example,

```
user@host $> mv file1.txt folder/file2.txt
```

  will move file `file1.txt` to the directory `folder` while changing its name to `file2.txt`. If you want to move a non-empty directory with all of its contents, use the `-r` flag.

- `g++` This commands compiles a C/C++ program. The default executable produced will have the name `a.out`, but a custom name can be given to the executable by using the `-o` flag,

```
user@host $> g++ code.cc -o executable_name
```

  The executable created can be run using

```
user@host $> ./executable_name
```

  To flush the standard output of the program to a file use the `>` command like so

```
user@host $> ./executable_name > output_file.dat
```

  To flush the error output of the program to a file use the `2>` command instead

```
user@host $> ./executable_name 2> error_log.txt
```

References

[Cummings et al., 2016] Cummings, A. C., Stone, E. C., Heikkila, B. C., Lal, N., Webber, W. R., Jóhannesson, G., Moskalenko, I. V., Orlando, E., and Porter, T. A. (2016). GALACTIC COSMIC RAYS IN THE LOCAL INTERSTELLAR MEDIUM: *VOYAGER 1* OBSERVATIONS AND MODEL RESULTS. *The Astrophysical Journal*, 831(1):18.

[De Angelis, 2011] De Angelis, A. (2011). Domenico Pacini, uncredited pioneer of the discovery of cosmic rays. *La Rivista del Nuovo Cimento*, 33(12):713–756.

[Fisk and Axford, 1969] Fisk, L. A. and Axford, W. I. (1969). Solar modulation of galactic cosmic rays, 1. *Journal of Geophysical Research*, 74(21):4973–4986.

[Hess, 2018] Hess, V. (2018). On the observations of the penetrating radiation during seven balloon flights. *arXiv*:1808.02927.

[Hörandel, 2013] Hörandel, J. R. (2013). Early cosmic-ray work published in german. In *AIP Conference Proceedings*, page 52–60. AIP.

[Kerr, 2013] Kerr, R. A. (2013). Radiation Will Make Astronauts' Trip to Mars Even Riskier. *Science*, 340(6136):1031–1031.

[Mace et al., 2000] Mace, R. L., Matthaeus, W. H., and Bieber, J. W. (2000). Numerical investigation of perpendicular diffusion of charged test particles in weak magnetostatic slab turbulence. *The Astrophysical Journal*, 538(1):192–202.

[Martucci et al., 2018] Martucci, M., Munini, R., Boezio, M., Felice, V. D., Adriani, O., Barbarino, G. C., Bazilevskaya, G. A., Bellotti, R., Bongi, M., Bonvicini, V., Bottai, S., Bruno, A., Cafagna, F., Campana, D., Carlson, P., Casolino, M., Castellini, G., Santis, C. D., Galper, A. M., Karelin, A. V., Koldashov, S. V., Koldobskiy, S., Krutkov, S. Y., Kvashnin, A. N., Leonov, A., Malakhov, V., Marcelli, L., Marcelli, N., Mayorov, A. G., Menn, W., Mergè, M., Mikhailov, V. V., Mocchiutti, E., Monaco, A., Mori, N., Osteria, G., Panico, B., Papini, P., Pearce, M., Picozza, P., Ricci, M., Ricciarini, S. B., Simon, M., Sparvoli, R., Spillantini, P., Stozhkov, Y. I., Vacchi, A., Vannuccini, E., Vasilyev, G., Voronov, S. A., Yurkin, Y. T., Zampa, G., Zampa, N., Potgieter, M. S., and Raath, J. L. (2018). Proton Fluxes Measured by the PAMELA Experiment from the Minimum to the Maximum Solar Activity for Solar Cycle 24. *The Astrophysical Journal Letters*, 854(1):L2.

[Parker, 1958] Parker, E. N. (1958). Dynamics of the Interplanetary Gas and Magnetic Fields. *The Astrophysical Journal*, 128:664.

[Zeitlin et al., 2013] Zeitlin, C., Hassler, D. M., Cucinotta, F. A., Ehresmann, B., Wimmer-Schweingruber, R. F., Brinza, D. E., Kang, S., Weigle, G., Böttcher, S., Böhm, E., Burmeister, S., Guo, J., Köhler, J., Martin, C., Posner, A., Rafkin, S., and Reitz, G. (2013). Measurements of Energetic Particle Radiation in Transit to Mars on the Mars Science Laboratory. *Science*, 340(6136):1080–1084.